Geotechnical Engineering
Volume 166 Issue GE5

Predicting ground movements in London Clay
Jurečič, Zdravković and Jovičić

ice | proceedings

Proceedings of the Institution of Civil Engineers
Geotechnical Engineering 166 October 2013 Issue GE5
Pages 466–482 http://dx.doi.org/10.1680/geng.11.00079
Paper 1100079
Received 27/08/2011 Accepted 16/04/2012
Published online 03/09/2012
Keywords: excavation/mathematical modelling/tunnels & tunnelling

ice Institution of Civil Engineers
publishing

Predicting ground movements in London Clay

1 **Nina Jurečič**
Research Assistant, Institute of Mining, Geotechnology and Environment (IRGO), Ljubljana, Slovenia

2 **Lidija Zdravković** MEng, MSc, PhD, DIC
Reader in Computational Soil Mechanics, Imperial College London, London, UK

3 **Vojkan Jovičić** MEng, MSc, PhD
Lecturer in Geotechnics, Institute of Mining, Geotechnology and Environment (IRGO), Ljubljana, Slovenia

The necessity of accounting for small-strain behaviour of soils in numerical analyses of the serviceability limit states of geotechnical structures is well established both nationally and internationally. This has led to further development of appropriate soil constitutive models, as well as to further advances in accurate laboratory measurements of small-strain stiffness. The current paper considers recent laboratory research into the behaviour of London Clay, performed at Imperial College in conjunction with the major ground works for Heathrow Terminal 5 in London, UK. This research has shown the small-strain response of London Clay to be different to that assumed previously and in particular to that determined from good-quality commercial experiments. Both sets of small-strain stiffness data are applied in this paper in finite-element analyses of a deep excavation and a tunnel construction in London Clay, with the objective of investigating their effect on predicted ground movements.

1. Introduction

Advanced laboratory testing of geotechnical materials has enhanced our understanding of many aspects of soil behaviour. Perhaps the most influential in recent years has been the recognition of soil's small-strain behaviour, which is characterised, among other features, by non-linearity of soil stiffness at small strains. A number of numerical studies of geotechnical problems (e.g. finite-element or finite-difference analyses) have shown that accounting for soil's non-linear stiffness improves the predictions of ground movements at serviceability limit states (e.g. Addenbrooke *et al.*, 1997; Higgins *et al.*, 1996; Hight and Higgins, 1994; Simpson *et al.*, 1996; Stallebrass *et al.*, 1994).

The constitutive modelling of small-strain behaviour of geotechnical materials has also evolved over the years, from simple non-linear elastic empirical models (e.g. Jardine *et al.*, 1986; Simpson *et al.*, 1979), to more advanced kinematic and bounding surface models that can reproduce, in addition to non-linearity and plasticity at early stages of loading, other advanced aspects of real soil behaviour (Baudet and Stallebrass, 2004; Grammatikopoulou *et al.*, 2006; Kavvadas and Amorosi, 2000; Manzari and Dafalias, 1997).

Recent laboratory-based research on the behaviour of London Clay, conducted at Imperial College and published largely in the *Géotechnique* 'Symposium in Print' 2007 (vol. 51, issue 1), was focused in part on the investigation of stiffness of natural London Clay (Gasparre *et al.*, 2007; Hight *et al.*, 2007). In particular, Hight *et al.* (2007) compared the stiffness decay curves of London Clay, from samples taken at various depths and in various lithological units, derived from earlier high-quality commercial laboratory testing and from this recent research, and showed that the two sets of results differ not only in the stiffness magnitude, but also in their decay in the small-strain range.

Considering that significant experience and confidence has been gained over the years in using the commercially derived stiffness decay curves in predictions of ground movements in London Clay (e.g. Higgins *et al.*, 1996; Kanapathipillai, 1996; Schroeder *et al.*, 2011; Simpson, 1992), the availability of the new, and significantly different, stiffness data for which there is no prior experience in predicting ground movements, raises the question as to which set of experimental evidence should be used in representing the stiffness of London Clay in future numerical analyses of geotechnical problems.

Hight *et al.* (2007) go some way to explain the reasons for the differences in the two sets of stiffnesses, but recognise that this needs further investigation. They also postulated that factors related to stiffness anisotropy may help to explain this anomaly,

considering that the commercial stiffness decay curves provided only isotropic stiffness, whereas Gasparre *et al.* (2007) contributed to further understanding of the small-strain stiffness anisotropy of London Clay. A subsequent study of Grammatikopoulou *et al.* (2008), on a shallow propped excavation in London Clay, indicated that there may be significant difference in predicted wall and ground movements around such an excavation when different sets of isotropic stiffness curves are used in analyses.

Based on the above, the objective of the current paper is to demonstrate the effects: (a) of the previous and the new isotropic small-strain stiffness data, and (b) of using anisotropic as opposed to isotropic small-strain stiffness data of London Clay on predictions of ground movements. Two boundary value problems are utilised for this purpose. The first one is the excavation of the Jubilee Line extension tunnels at St James's park, for which there are measurements of ground movements due to tunnel excavations that can be compared to numerical predictions (i.e. class C analyses according to Lambe (1973)). The second example is a deep excavation at Moorgate, on the Crossrail route, which has not yet been constructed and hence the numerical predictions are before the event (i.e. class A analyses). It is further emphasised that in each of the two studies all other numerical details (e.g. initial stresses, permeability, constitutive models and boundary conditions) are the same, only the small-strain stiffness of London Clay is varied. Also, the initial stresses in the ground in each of the two studies correspond to equilibrium greenfield conditions when the depositional history of all the layers is completed. In terms of the non-linear small-strain behaviour this means that the stiffness in the soil starts from a respective elastic plateau and then degrades with the increase in strain level due to the construction of tunnels or deep excavation respectively. All analyses have been performed using the finite-element software ICFEP (Potts and Zdravković, 1999), which employs the modified Newton–Raphson method with an error-controlled sub-stepping stress-point algorithm as its non-linear solver.

2. Calibration of constitutive models

Considering the objectives of this study, the main emphasis in the calibration process has been on the small-strain stiffness of London Clay, adopting the same modelling framework for both the old and the new stiffness data. The chosen constitutive model is a form of a non-linear elastic and non-associated plastic Mohr–Coulomb model (Potts and Zdravković, 1999). The non-linearity below the Mohr–Coulomb yield surface accounts for stiffness variation with both stress and strain levels. The isotropic non-linear model allows independent input of the shear and the bulk stiffness parameters, according to the Jardine *et al.* (1986) non-linear expression given in the Appendix. The anisotropic stiffness model, developed by Franzius *et al.* (2005), adopts similar expressions for non-linear stiffness variation (see Appendix), but the bulk stiffness is not an independent input.

2.1 Available stiffness data

The shear stiffness data for the London Clay used for calibration are reproduced in Figure 1 from Hight *et al.* (2007). This figure shows the normalised secant undrained Young's modulus, E_u/p', plotted against axial strain, ε_a, from recent undrained triaxial compression tests on samples of London Clay from the Heathrow Terminal 5 site, from a range of depths and lithological units (Gasparre, 2005). Also shown in the figure is a range of stiffnesses obtained in the past from high-quality commercial tests. The new set of data shows a narrow range of stiffness variation and very gradual stiffness decay. On the other hand, the previously established bounds for London Clay indicate higher magnitudes of stiffness, no clear plateau, a bigger range of variation and also a more rapid decay.

The secant bulk stiffness data for the London Clay are reproduced in Figure 2 from Hight *et al.* (2007). These data are also obtained from recent experiments on samples of London Clay from Heathrow Terminal 5. In particular, the bulk stiffness is obtained from the recompression stages of the triaxial tests, during reconsolidation to in situ stresses (Gasparre, 2005). The figure plots the normalised bulk stiffness curves, K/p', from various lithological units against the volumetric strain, ε_{vol}. The scatter in the figure indicates the difficulties in measuring volumetric strains in an experiment, either from external or internal gauges.

2.2 Calibration of isotropic stiffness

The calibrated normalised secant shear and bulk stiffness curves are plotted together with the experimental data in Figures 1 and 2 respectively. It should be noted that for an isotropic model $E_u = 3G$.

The two shear stiffness curves in Figure 1, marked as 'Previous stiff' and 'Previous soft', have been calibrated in the past on

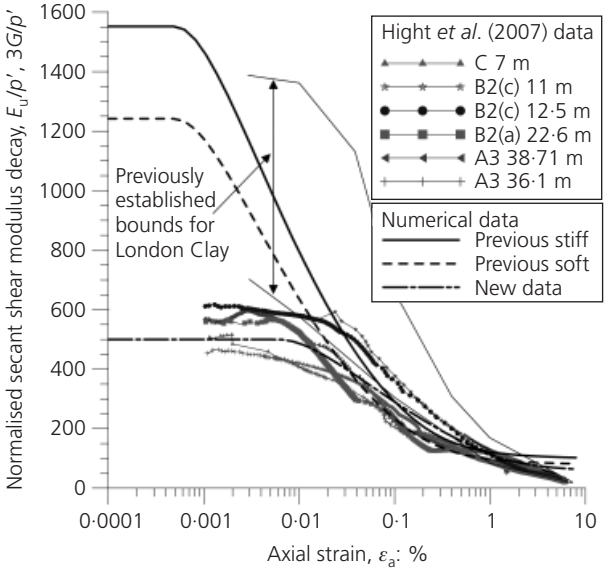

Figure 1. Normalised secant shear stiffness of London Clay (data after Hight *et al.*, 2007)

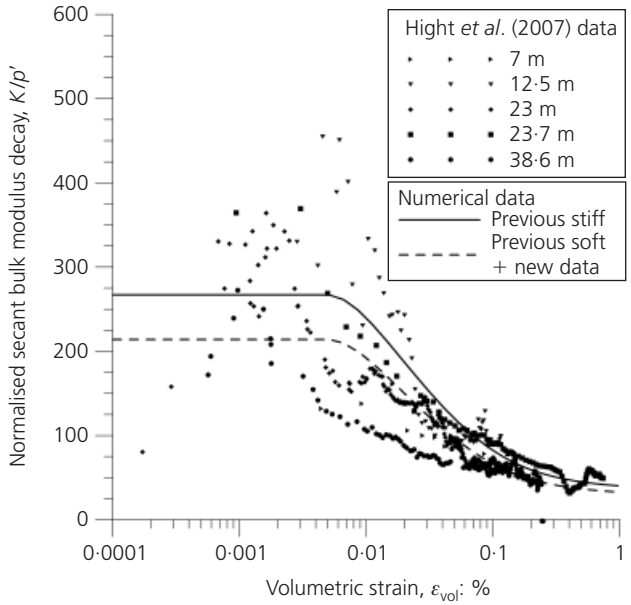

Figure 2. Normalised secant bulk stiffness data of London Clay (data after Hight *et al.*, 2007)

some of the commercial experiments and were adopted in the numerical studies presented by Zdravković *et al.* (2005) and Addenbrooke *et al.* (1997) respectively. Therefore, they were not calibrated in this study and the appropriate parameters for the non-linear stiffness model are summarised in Table 1. It is evident from the figure that these two curves fall into the previously established range for London Clay at axial strain levels between 0·005% and 0·05%. At larger strain levels they plot below this range, falling back into the range for strains between 0·5% and 1%. There is no indication from the previous data in Figure 1 about the stiffness values at strains less than 0·001%.

The isotropic secant shear stiffness calibrated from the new data of Hight *et al.* (2007) is shown as a dot-dashed line in Figure 1, whereas the corresponding parameters for the non-linear stiffness model are summarised in Table 1. This curve plots approximately as an average of experimental data, with the elastic plateau chosen at $E_u/p' = 500$.

Similar to Figure 1, Figure 2 shows the 'Previous stiff' and the 'Previous soft' normalised secant bulk stiffness curves calibrated from previous experiments and used in the studies of Zdravković *et al.* (2005) and Addenbrooke *et al.* (1997). The parameters for the non-linear model for both curves are summarised in Table 2. It is evident from Figure 2 that both curves plot within the experimental data, although the 'Previous stiff' curve is on a higher side in the range of 0·05 to 1·0% of the volumetric strain. The curves also have similar rate of degradation, but different plateaus.

Owing to the large scatter in the Hight *et al.* (2007) data in Figure 2, in particular for volumetric strains smaller than 0·01%, no new calibration of these data has been performed. Instead it was considered that the 'Previous soft' curve averages the experimental data reasonably well and hence the 'new' curve for the secant bulk modulus was chosen to be the same as this curve.

Finally, for completeness, because the numerical software utilises the tangent, rather than the secant stiffness, the isotropic secant shear stiffness curves from Figure 1 are shown in their tangent form in Figure 3, whereas the isotropic secant bulk stiffness curves from Figure 2 are shown in their tangent form in Figure 4.

2.3 Calibration of anisotropic stiffness

The shear stiffness of London Clay has long been recognised as anisotropic, due to its significant overconsolidation caused by the

Shear stiffness	A	B	$C \times 10^{-4}$: %	α	γ	$\varepsilon_{d,min} \times 10^{-4}$: %	$\varepsilon_{d,max}$: %	G_{min}: kPa
Original stiff	1400	1270	1	1·335	0·617	8·66025	0·6928	2667
Original soft	1120	1016	1	1·335	0·617	8·66025	0·6928	2667
New data	350	330	30	1·336	0·617	107·39	1·732	2667

Table 1. Shear stiffness parameters for London Clay for isotropic non-linear elastic model (see Appendix)

Bulk stiffness	R	S	$T \times 10^{-3}$: %	δ	η	$\varepsilon_{vol,min} \times 10^{-3}$: %	$\varepsilon_{vol,max}$: %	K_{min}: kPa
Original stiff	686	633	1	2·069	0·420	5·0	0·15	5000
Original soft	549	506	1	2·069	0·420	5·0	0·15	5000
New data	549	506	1	2·069	0·420	5·0	0·15	5000

Table 2. Bulk stiffness parameters for London Clay for isotropic non-linear elastic model (see Appendix)

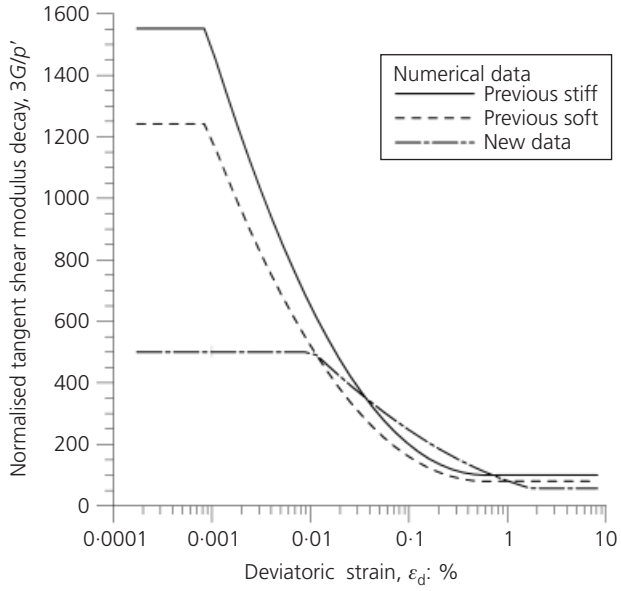

Figure 3. Normalised tangent shear stiffness of London Clay

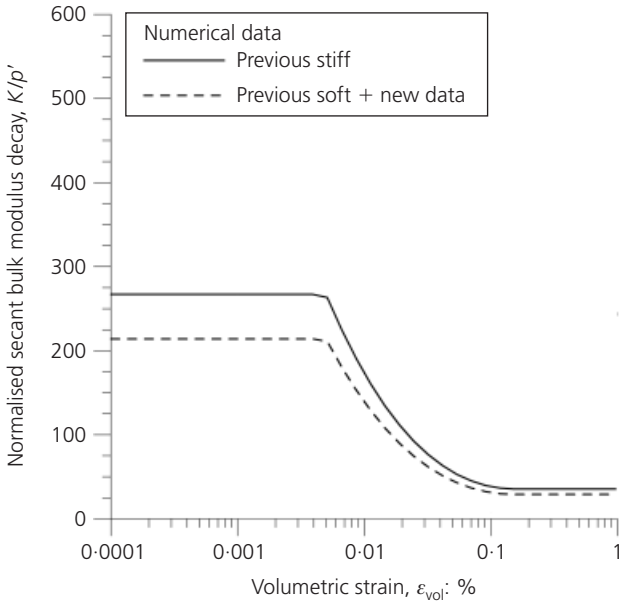

Figure 4. Normalised bulk stiffness of London Clay

geological erosion of approximately its top 200 m. In general, the horizontal component of stiffness is larger than the vertical. The new experimental data of Gasparre (2005) and Gasparre *et al.* (2007) contribute to the understanding of the elastic stiffness anisotropy. In these experiments various components of elastic stiffness were measured with bender elements and triaxial probing tests on samples of London Clay from Heathrow Terminal 5. However, this work does not provide information as to how anisotropy develops with strain level. Therefore, certain assumptions had to be applied in deriving anisotropic stiffness curves for the analyses presented in this paper. Since there are no other data, only the tangent stiffness curves will be derived in this part, as this is the required input for the numerical software.

For the calibration of the very small-strain elastic stiffness properties (i.e. the plateau values) the relevant data from Gasparre (2005) and Gasparre *et al.* (2007) are reproduced in Figure 5, which shows the variation of these properties with depth/lithological units. The non-linear anisotropic model of Franzius *et al.* (2005) is based on a three-parameter cross-anisotropic formulation of Graham and Houlsby (1983), which is valid for the plateau part of the stiffness curves, combined with a non-linear elastic response beyond the plateau. The three independent parameters required for this cross-anisotropic formulation are: the drained Young's modulus E'_v (in the vertical direction), the drained Poisson ratio μ'_{hh} for horizontal strain due to horizontal strain and the anisotropic scale factor α ($= \sqrt{E'_h/E'_v} = G_{hh}/G_{vh} = \mu'_{hh}/\mu'_{vh}$). All other cross-anisotropic parameters are calculated from this input as explained in the Appendix. In the equalities for α given above, E'_h is the drained Young's modulus in the horizontal direction, G_{hh} and G_{vh} are the shear moduli in the horizontal and vertical plane respectively and μ'_{vh} is the drained Poisson ratio for vertical strain due to horizontal strain.

2.3.1 Calibration approach 1 (Cal1)

The calibration in this approach is based on the 'new' E_u/p' modulus decay curve calibrated in Figure 1, utilising its tangent form given in Figure 3. Using the laboratory data on elastic stiffness parameters presented in Figure 5, the average ratio with depth of the undrained and drained Young's moduli in the vertical direction, E_u/E'_v, is estimated to be 1·6 from Figures 5(a) and 5(f). The whole 'new' tangent modulus decay curve E_u/p', shown again in Figure 6(a), is divided by 1·6, thus producing the normalised tangent E'_v/p' curve shown as a line with crosses in Figure 6(a). This curve is an input for the anisotropic non-linear model and the calibrated model parameters are summarised in Table 3.

Further to this, the ratio of the drained horizontal and vertical Young's moduli, E'_h/E'_v, is estimated from Figures 5(a) and 5(e) to be about 2·2 on average. Therefore, the input parameter for the model, α, is taken as 1·5. The normalised horizontal stiffness curve E'_h/p', shown as a grey solid line in Figure 6(a), results from multiplication of the E'_v/p' curve by 2·2 (i.e. the elastic stiffness ratio is assumed constant over the whole strain range). If an undrained triaxial compression test is now performed numerically, using the anisotropic small-strain stiffness model, the resulting equivalent E_u/p' stiffness curve (solid black line) is different from the 'new' E_u/p' curve from which the anisotropic stiffness is derived. Although this may look anomalous, it is a result of the scatter in the elastic data in Figure 5 from which the adopted values are averaged. The distribution with depth of the so-determined equivalent elastic values of E_u in Figure 5(f) still

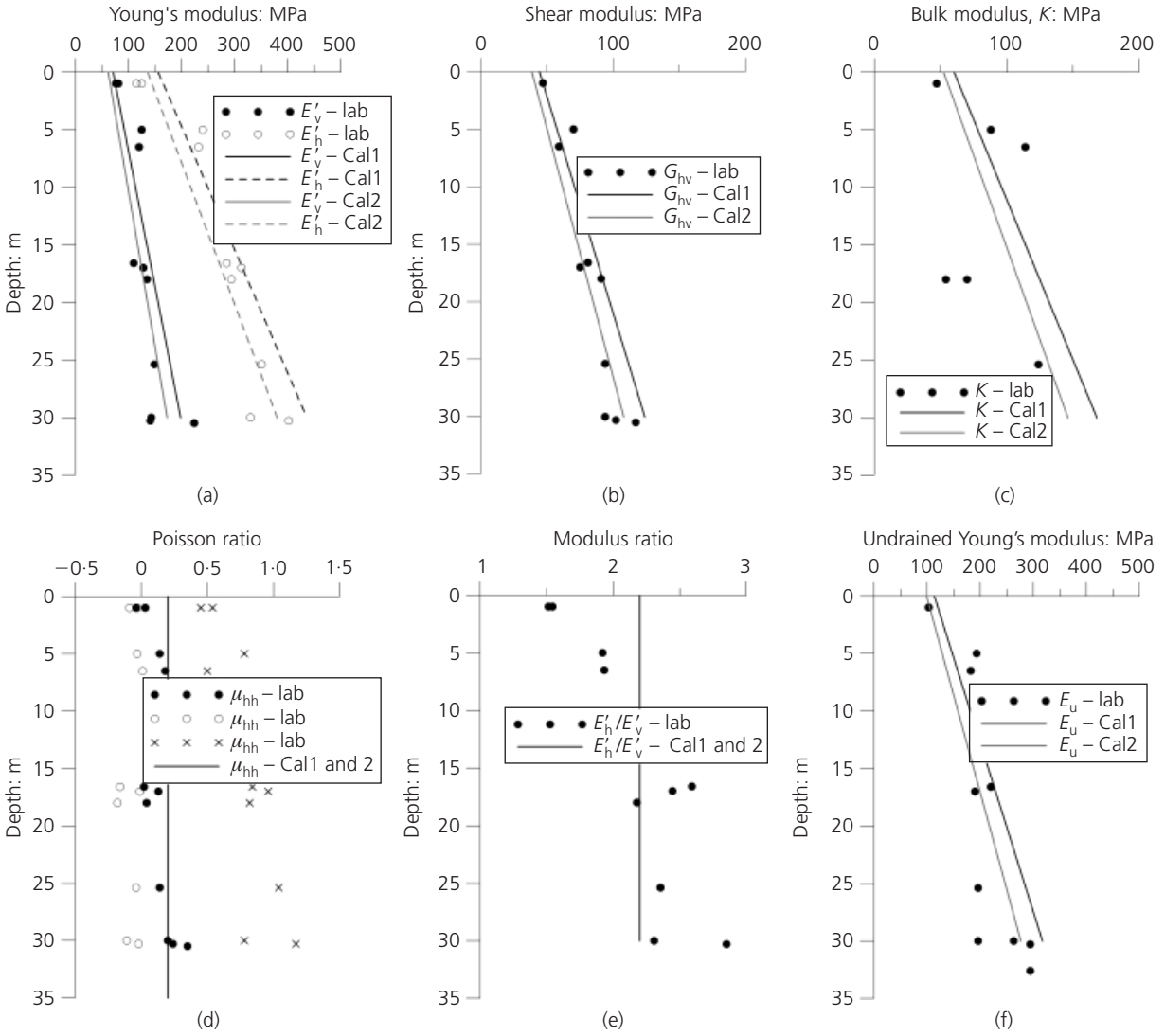

Figure 5. Profiles of elastic stiffness parameters (data after Gasparre *et al.* (2007)

plots within the bounds of experimental data (solid black line, E_u – Cal1). The same is valid for the profiles of elastic values of E'_v and E'_h in Figure 5(a) (the pair of solid and dashed black lines), as well as for the elastic values of G_{vh} in Figure 5(b) (the solid black line), which all plot within the experimental data.

As noted earlier, the bulk stiffness in this model is not an independent input. The resulting normalised tangent bulk stiffness curve for this calibration approach, obtained from simulating an isotropic compression test with the above non-linear anisotropic model parameters, is shown in Figure 7. The resulting distribution with depth of the elastic bulk modulus is shown in Figure 5(c). Although the experimental evidence is sparse, the numerical data are broadly within the measured range. In comparison with the curves shown in Figure 4, the magnitudes of the elastic very small-strain normalised bulk stiffness are similar (i.e. within the 200–300 range), but the elastic plateau itself is longer and the decay is more gradual.

Since there is no experimental evidence to suggest that the elastic stiffness anisotropy maintains the same E'_h/E'_v ratio at higher strains, an additional option is introduced in which this ratio varies from its maximum elastic value (2·2 in this case) at the end of the elastic plateau, to unity at the end of the non-linear variation of stiffness. The resulting E'_h (and E_u) degradations in the non-linear range are shown as dashed lines in Figure 6(a). All other model parameters are the same as in the case of the constant ratio.

2.3.2 Calibration approach 2 (Cal2):

The 'new' E_u/p' curve from Figure 3 is also the basis of this calibration approach, reproduced again in Figure 6(b). However,

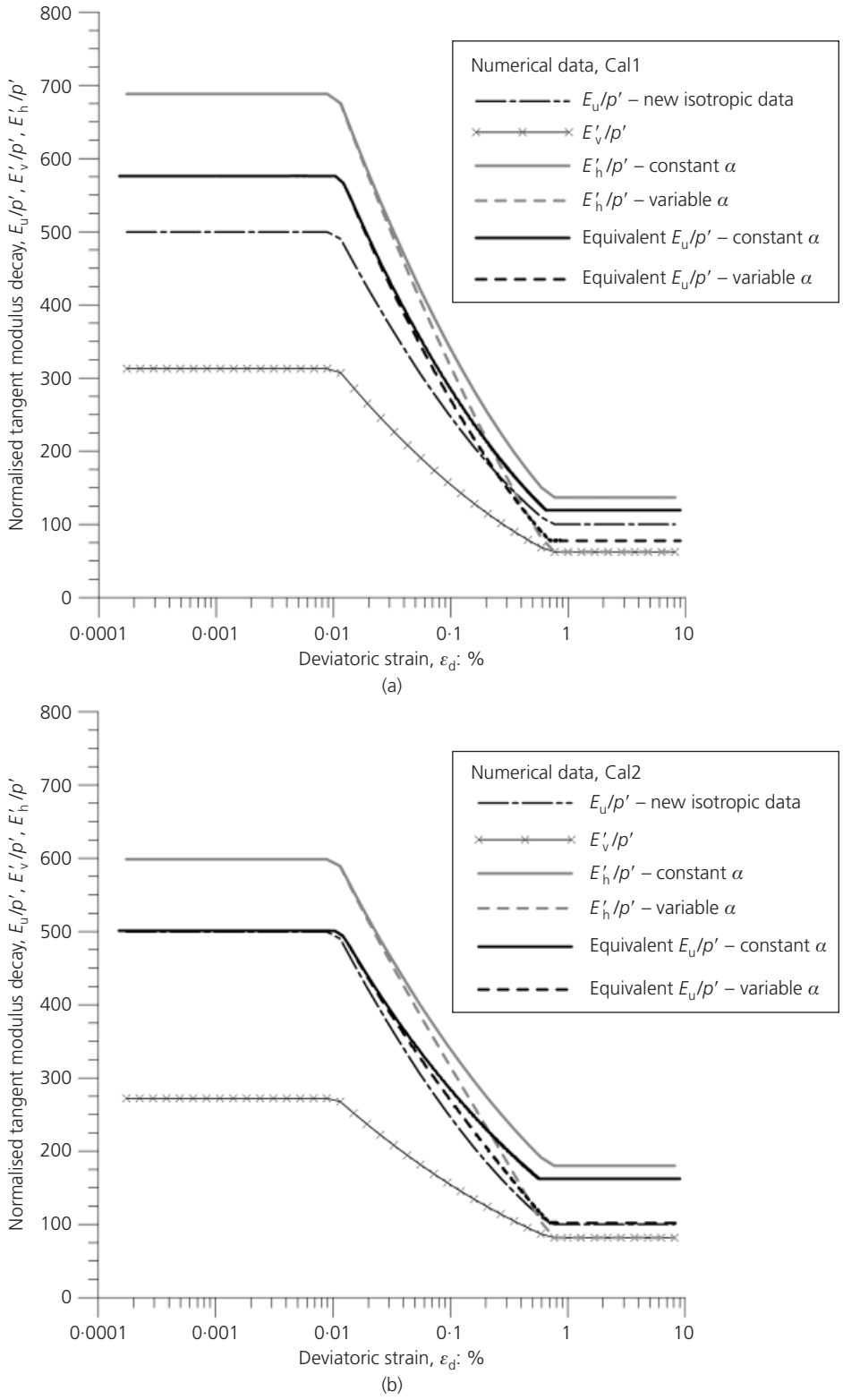

Figure 6. Calibration for the non-linear anisotripic model: (a) Cal1 and (b) Cal2

Parameters	P	Q	D: %	β	ξ	$\varepsilon_{d,min} \times 10^{-4}$: %	$\varepsilon_{d,max}$: %	$E'_{v,min}$: kPa
Cal1	219	207	0·0030	1·336	0·617	107·39	0·6928	2000
Cal2	200	190	0·0025	1·3	0·55	107·39	0·6928	2000

Table 3. E_v' stiffness parameters for London Clay for anisotropic non-linear elastic model (see Appendix)

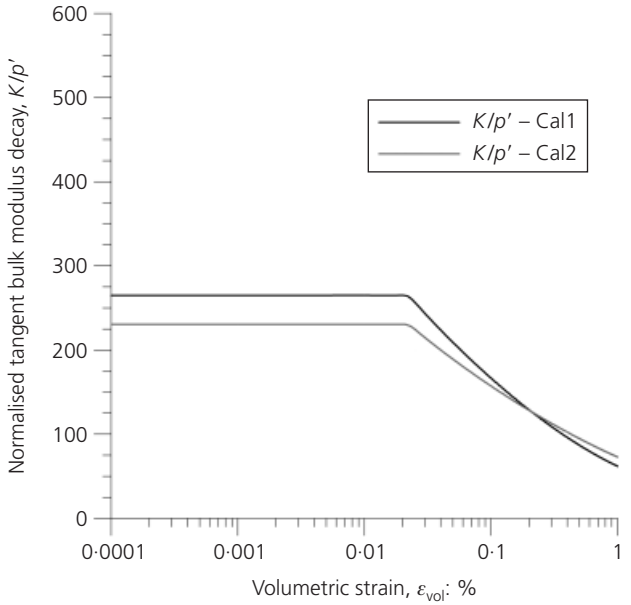

Figure 7. Resulting bulk stiffness curves from Cal1 and Cal2 calibration approaches, of the anisotropic non-linear stiffness model

the calibration is now performed in such a way that the numerical, undrained, triaxial compression test using the anisotropic, non-linear, elastic model results in a similar equivalent E_u/p' curve as that calibrated from the 'new data'. This is an iterative process in which the same $E'_h/E'_v = 2{\cdot}2$ ratio is adopted in the plateau range, while its variation from 2·2 to 1·0 is adopted in the non-linear degradation range. The resulting equivalent E_u/p' curve is shown as a black dashed line in Figure 6(b) and the corresponding E'_v/p' and E'_h/p' curves are shown as a line with crosses and a grey dashed line respectively.

If a constant ratio $E'_h/E'_v = 2{\cdot}2$ is adopted in the whole strain range, then the resulting equivalent E_u/p' curve deviates significantly from the calibrated 'new' curve in the non-linear range and at higher strain levels (black solid line) and the corresponding E'_h/p' curve is shown as a grey solid line in Figure 6(b). It is not possible to calibrate the model such that the same equivalent E_u/p' curve is obtained for both the constant and the variable E'_h/E'_v ratio and for the same E'_v/p' curve. The parameters for the non-linear anisotropic model for this curve are summarised in Table 3.

Comparing Figures 6(a) and 6(b) it is evident that the very small-strain elastic values of the directional stiffnesses (i.e. E'_v/p' and E'_h/p') are lower with this calibration procedure compared to those obtained with the Cal1 approach. Therefore, their profiles with depth in Figure 5(a) (a pair of grey solid and dashed lines) plot to the left of the equivalent profiles from the Cal1 calibration, but still within the experimental data. A similar result is obtained for the elastic profiles of G_{vh} in Figure 5(b), E_u in Figure 5(f) and K in Figure 5(c). The resulting K/p' stiffness curve from this calibration is shown in Figure 7, plotting very closely to the curve from the Cal1 calibration.

3. Boundary value problem 1: Jubilee Line tunnels at St James's park

3.1 Geometry and ground conditions

The first geotechnical problem considered in this study is the excavation of the Jubilee Line tunnels at St James's park in London in 1996, as part of the Jubilee Line extension project (Standing *et al.*, 1996). This is a greenfield site where the westbound (WB) tunnel was excavated first, followed by the eastbound tunnel (EB) 8 months later, both within the London Clay formation. The geometry of the problem and the ground profile are shown in Figure 8. Other ground conditions include a hydrostatic pore water pressure profile from the top of Terrace Gravel and a K_o profile of 1·5 magnitude in the London Clay formation and 0·5 in the layers above it.

The difficulty of predicting accurately settlement troughs in high K_o soils, such as London Clay, is well known and a number of previous numerical studies (e.g. Addenbrooke *et al.*, 1997; Franzius *et al.*, 2005) have shown that this is also the case for the St James's park tunnels. An additional issue for this case study is the high volume loss observed on site, with 3·3% and 2·9% quoted respectively for the WB and EB tunnels (Standing *et al.*, 1996), which is much higher than the expected value of up to 1·0–1·5%, based on past experience.

3.2 Numerical modelling

Coupled consolidation plane strain analyses have been performed in the current paper to investigate both the short- and long-term ground movements around the tunnels, utilising both the isotropic and anisotropic stiffness properties for London Clay presented in the previous section. The remaining soil layers are modelled in the same manner and with the same model parameters as in the study of Addenbrooke *et al.* (1997), hence their calibration is not

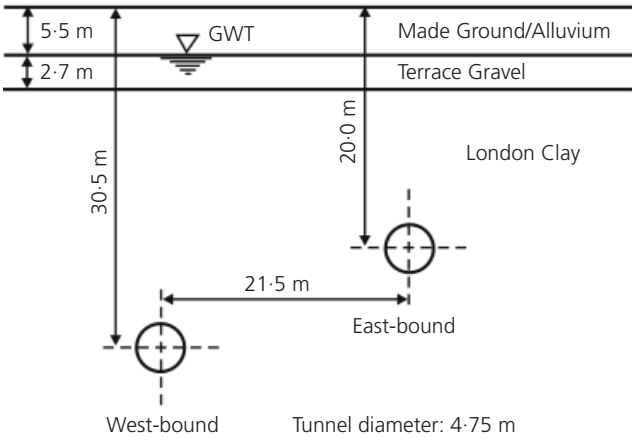

Figure 8. Geometry and ground conditions at St James's Park (after Addenbrooke *et al.*, 1997)

presented here. The made ground is modelled as a linear elastic material, whereas the terrace gravel is modelled with the same isotropic non-linear elastic Mohr–Coulomb model as applied in the modelling of the London Clay. For simplicity, the tunnel linings are modelled as elastic rings, with appropriate cross-sectional properties. The parameters for all materials are summarised in Tables 4–6. It should be noted that the analyses of Addenbrooke *et al.* (1997) of this case study employed stiffness properties of London Clay which correspond to the 'previous soft' isotropic curves in Figures 3 and 4.

The finite-element mesh for this problem is shown in Figure 9. It utilises eight-noded isoparametric quadrilateral elements to discretise the soil and three-noded beam elements to represent tunnel linings. The construction sequence involves first the excavation of the WB tunnel under undrained conditions (by prescribing small time steps), followed by a rest period of 8 months during which partial dissipation of excess pore-water pressures occurs, then an undrained excavation of the EB tunnel (again prescribing small time steps) and subsequent long-term consolidation until the complete dissipation of excess pore-water pressures. The 'volume loss' modelling procedure is applied (see e.g. Potts and Zdravković, 2001) to ensure that the observed volume losses are achieved numerically. Each tunnel is excavated over 40 increments and

Layer	Angle of shearing resistance, ϕ': deg	Cohesion, c': kPa	Angle of dilation, ψ: deg	Stiffness: kPa	Poisson ratio, μ	Permeability, k_o: m/s
Made Ground	—	—	—	5000·0	0·3	Drained
Terrace Gravel	35·0	0·0	17·5	Small strains (Table 5)	0·2	Drained
London Clay	22·5	5·0	11·25	Small strains (Tables 1–3)	0·2	2×10^{-9}[a]

[a] See Appendix for the permeability model.

Table 4. Mohr–Coulomb parameters for soils in St James's park tunnel analyses

Shear stiffness	A	B	$C \times 10^{-4}$: %	α	γ	$\varepsilon_{d,min} \times 10^{-4}$: %	$\varepsilon_{d,max}$: %	G_{min}: kPa
Terrace Gravel	1380	1248	5	0·974	0·940	8·83346	0·3464	2000
Bulk stiffness	R	S	$T \times 10^{-3}$: %	δ	η	$\varepsilon_{vol,min} \times 10^{-3}$: %	$\varepsilon_{vol,max}$: %	K_{min}: kPa
Terrace Gravel	275	225	2	0·998	1·044	2·1	0·2	5000

Table 5. Shear stiffness parameters for isotropic non-linear elastic model for Terrace Gravel in St James's park analyses (see Appendix)

Young's modulus, E: kPa	Poisson ratio, μ	Cross-sectional area, A: m^2	Second moment of inertia, I: m^4
$28{\cdot}0 \times 10^6$	0·15	0·2	$6{\cdot}667 \times 10^{-4}$

Table 6. Parameters for tunnel lining linear elastic model in St James's park analyses

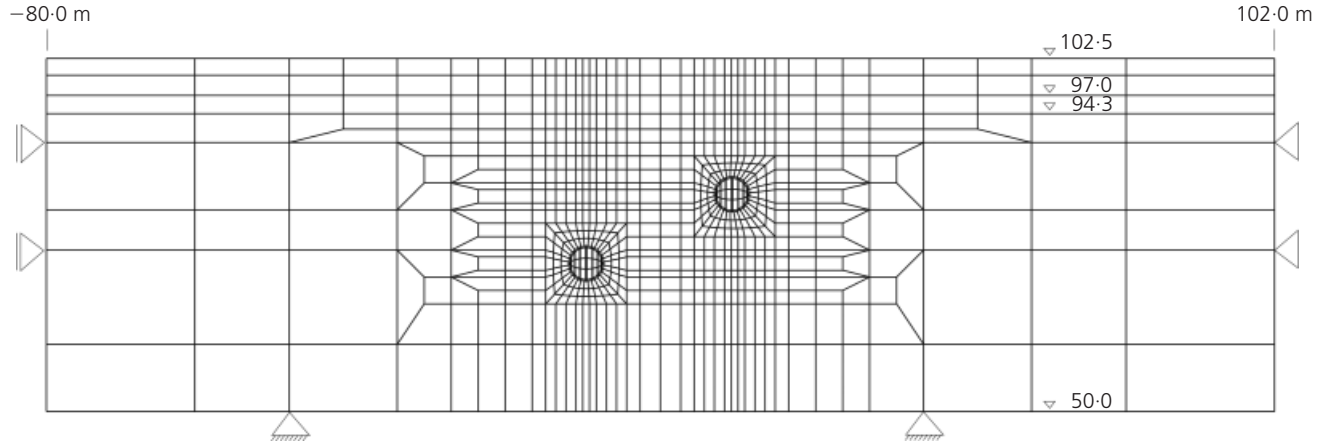

Figure 9. Finite-element mesh for St James's Park analyses

when the desired volume loss is achieved the tunnel lining is constructed. Because of the high volume loss, a high ground unloading had to be applied before lining construction, which was about 80% on average for both tunnels.

The boundary conditions applied to the mesh are those of zero horizontal and vertical displacements at the bottom boundary, as well as zero horizontal displacements and zero vertical forces on the vertical boundaries. As the analyses are coupled, hydraulic boundary conditions are also needed, which in this case involve no change of pore pressures along the vertical and the bottom boundaries of the London Clay and drained behaviour of the Made Ground and Terrace Gravels. In addition, when each of the tunnel linings is installed, the precipitation boundary condition is applied on the whole tunnel boundary. This boundary condition automatically applies either a zero flow (compatible with short-term tunnel behaviour) or a zero pore pressure (compatible with the long-term tunnel behaviour) boundary condition at nodes of the tunnel boundary (Potts and Zdravković, 1999).

3.3 Results – short term

The results from the excavation of the WB tunnel are considered first, as this is the first excavation on site. Since it is performed under predominantly undrained conditions, it is the shear stiffness properties of the soil that govern the ground response. Figure 10 shows the surface settlement troughs immediately after the construction of the tunnel lining, resulting from the analyses utilising isotropic shear stiffness properties of London Clay shown in Figure 3. The analyses with the two 'previously' derived shear stiffness curves result in almost identical settlement troughs, with a maximum settlement above the WB tunnel of 10·5 mm. The isotropic shear stiffness curve calibrated from the new data of Hight *et al.* (2007) results in a wider and shallower settlement trough, with the maximum settlement of about 8 mm.

For clarity, the resulting settlement troughs from analyses employing the anisotropic small-strain non-linear model (with stiffness curves from Figure 6) are shown separately in Figure 11. For comparison, the settlement trough from the isotropic 'new data' is also shown, as the anisotropic stiffness curves have been derived from the 'new' isotropic stiffness. It is evident that such modelling of London Clay results in marginally narrower settlement troughs and higher maximum settlements, but these are still smaller than those predicted by the 'previous' isotropic stiffness curves in Figure 10. It is also evident that the calibration procedure Cal1 results in a combination of anisotropic stiffness which produces larger settlements than the anisotropic stiffness resulting from the Cal2 calibration procedure. However, the influence of how the stiffness ratio E'_h/E'_v varies with strain is not very large, although the combination with the varying stiffness ratio produces marginally larger settlements from both calibration procedures.

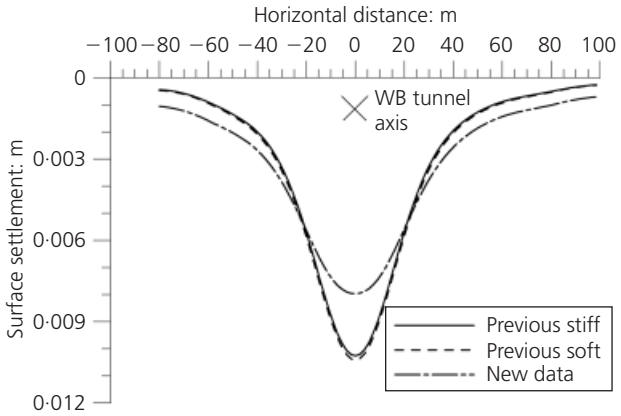

Figure 10. Predicted short-term settlement troughs above the WB tunnel using isotropic small-strain stiffness properties

Although the maximum difference in predicted maximum settlements from all analyses is about 20% (8–10 mm), these are on

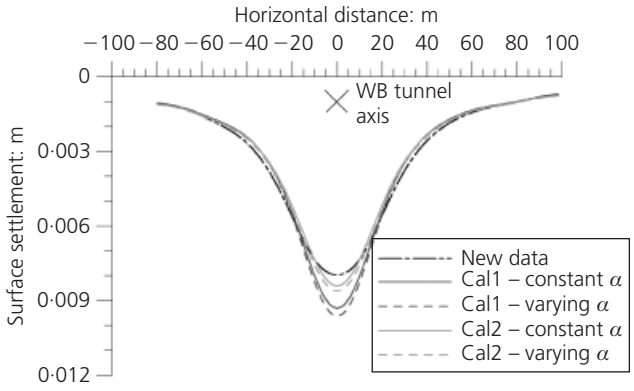

Figure 11. Predicted short-term settlement troughs above the WB tunnel using anisotropic small-strain stiffness properties

average only about half of the observed maximum settlement of 20 mm. The slight differences between the predicted settlements can be explained partly by the mobilised levels of elastic deviatoric strain, ε_d, around the WB tunnel in each analysis. In this respect, Figure 12 shows the mobilised ε_d strain in the soil in the WB tunnel vertical axis directly above the crown (Figure 12(a)) and along its spring line (Figure 12(b)), for the conditions in the soil when 1% and 3·3% volume loss is reached. These figures show that even at 1% volume loss, the mobilised ε_d is already in the range of 0·01 to 1·0%. The indication is therefore that the shear stiffness degrades very quickly from the beginning of tunnel excavation and this strain range remains operational until the final volume loss of 3·3% is achieved. In this range the 'previously' derived shear stiffness curves in Figure 3 have steeper degradation and lower shear stiffness values compared to the 'new' isotropic shear stiffness, which has a much more gradual decay, thus resulting in smaller settlements. A similar observation is valid for the anisotropic stiffness curves whose settlement predictions plot in between the two extreme values of isotropic predictions.

To show more clearly the differences in settlement troughs from all analyses and from the measured trough, the normalised settlement troughs (i.e. settlements of each trough normalised by the maximum settlement of that trough) are shown in Figure 13 for comparison.

Figure 14 presents the total surface settlement profiles immediately after the construction of the EB tunnel (i.e. total movements mobilised from the beginning of analysis, including both tunnel excavations and the 8-month rest period in between). In general, the settlement troughs have moved to the right of the WB tunnel axis, with maximum settlements being in between the two tunnel axes and about twice as large compared to the corresponding settlements immediately after the WB tunnel construction. In terms of the different analyses, comparing Figures 10, 11 and 14, the smallest settlement is still predicted using the 'new' isotropic

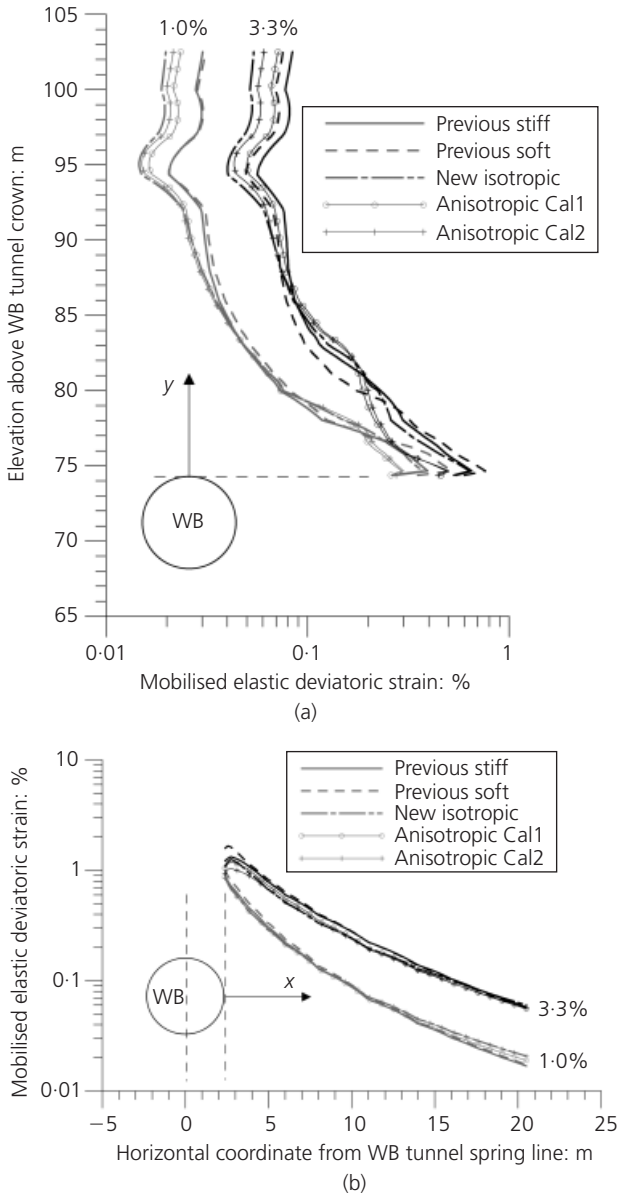

Figure 12. Mobilised elastic deviatoric strain: (a) above the crown along the tunnel axis and (b) along the tunnel spring line

stiffness, whereas the largest settlements are predicted by the 'previous' isotropic stiffness curves.

3.4 Results – long term

After the construction of the EB tunnel is completed, a period of time is simulated in all analyses to allow full dissipation of excess pore-water pressures, thus allowing an assessment of long-term ground movements above the tunnels. The predicted long-term settlement troughs from all analyses are shown in Figure 15. It should be noted that for this analysis stage both the shear and the bulk stiffness and their variation with stress and strain levels affect the soil behaviour.

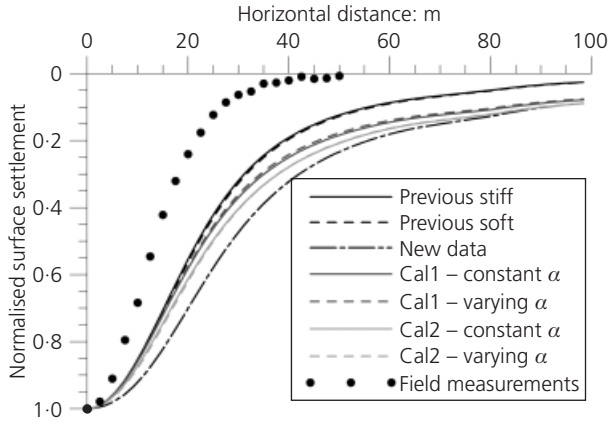

Figure 13. Normalised settlement troughs above the WB tunnel from all analyses

In general, the maximum settlements in Figure 15 are 3–4 times larger than the maximum short-term settlements predicted above the WB tunnel. This is broadly in agreement with what was measured on site, where the consolidation settlement is reported to be about 4 times larger than the short-term settlement (Mair, 2008). However, the absolute magnitudes of long-term settlements are still underpredicted and the introduction of the newly derived isotropic and anisotropic shear stiffness does not appear to significantly affect the predictions, compared to those obtained using the previously established data. The maximum difference between the largest (46·1 mm) and the smallest (34·3 mm) predicted maximum settlement is 26%. The order of some predictions has also changed from short to long term, indicating the interaction of the shear and bulk stiffness.

4. Boundary value problem 2: Moorhouse excavation

4.1 Geometry and ground conditions

This boundary value problem involves a deep excavation at Moorgate in London, on the route of the future Crossrail tunnels, known as the Moorhouse excavation. It is planned to serve as a launching chamber for Crossrail tunnel excavation and subsequently as part of a station hall. The geometry of the excavation, which is 40 m deep and involves several levels of propping, and the ground profile are shown in Figure 16. The details of the ground conditions (i.e. pore-water pressure and K_o profiles) applied in the analyses presented here are given in Zdravković *et al.* (2005) and are not repeated in the current paper, for the sake of brevity.

4.2 Numerical modelling

Coupled consolidation plane strain analyses have also been performed for this problem, investigating both the short- and long-term ground movements around the excavation, utilising both isotropic and anisotropic stiffness properties for London Clay as in the tunnelling analyses. The remaining soil layers are modelled with the same constitutive models and model parameters as in the study of Zdravković *et al.* (2005), hence their calibration is not repeated here. The Made Ground is modelled as a linear elastic material, whereas the Terrace Gravel and Thanet Sand are modelled with the isotropic non-linear elastic Mohr–Coulomb model. All soils are discretised with eight-noded quadrilateral elements. The props (modelled with two-noded bar elements) and the wall (modelled with three-noded beam elements which are placed on the excavation side of the actual wall in Figure 16) are also considered elastic. The parameters for all materials are summarised in Tables 7–9. It should be noted that the study of Zdravković *et al.* (2005) employed stiffness proper-

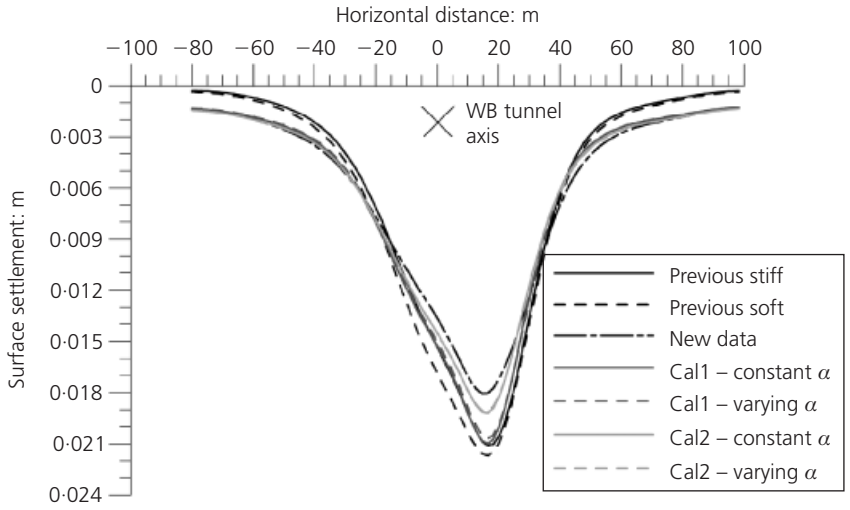

Figure 14. Predicted surface settlement troughs after the construction of the EB tunnel

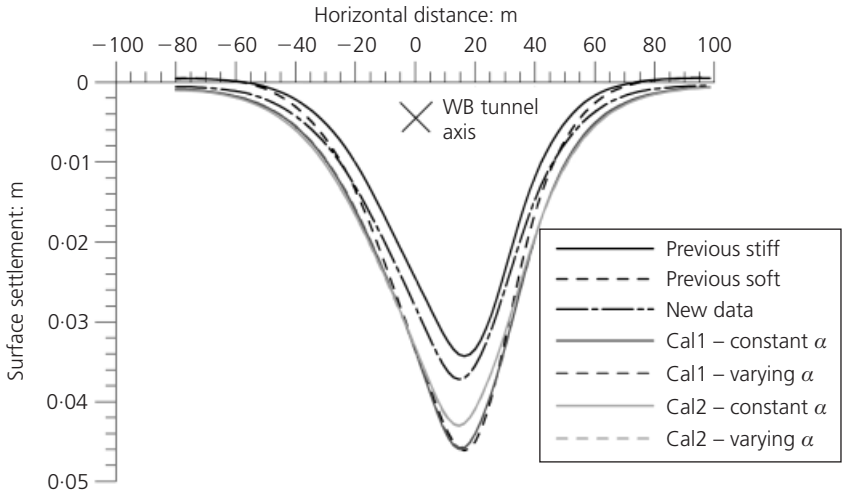

Figure 15. Predicted long-term settlement troughs

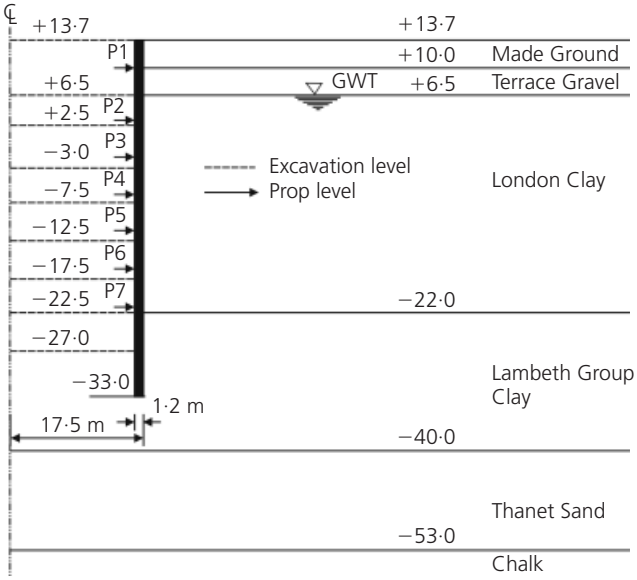

Figure 16. Geometry and ground conditions of the Moorhouse excavation (after Zdravković *et al.*, 2005)

ties of London Clay for this site which correspond to the 'previous stiff' curves in Figures 3 and 4.

The construction sequence (see Figure 16) involves consecutive excavation of soil (the dashed lines indicate various excavation levels) followed by the construction of a prop, until the final excavation level at −27 m elevation is reached and all props are installed. It is assumed that the wall acts as a cantilever during the first excavation stage to +6·5 m elevation, before the prop P1 is installed. The excavation is modelled as undrained by applying small time steps.

The boundary conditions applied to the mesh are those of zero horizontal and vertical displacements at the bottom boundary, as well as zero horizontal displacements and zero vertical forces on the vertical boundaries. The Made Ground, Terrace Gravels and Thanet Sand are considered as drained materials and a zero change of pore-water pressure is prescribed in the clays on the right-hand side vertical boundary. A no flow of water boundary condition is assumed at the axis of symmetry. After the final excavation stage is performed, a zero pore-water pressure boundary condition is applied along the excavation boundary in the long term.

Layer	Angle of shearing resistance, ϕ': deg	Cohesion, c': kPa	Angle of dilation, ψ: deg	Stiffness: kPa	Poisson ratio, μ	Permeability, k_o: m/s
Made Ground	25·0	0·0	12·5	10000·0	0·2	Drained
Terrace Gravel	35·0	0·0	17·5	Small strains (Table 8)	0·2	Drained
London Clay	22·0	0·0	11·0	Small strains (Tables 1–3)	0·3	1×10^{-9}
Lambeth Group Clay	22·0	0·0	11·0	Small strains (Tables 1–3)	0·3	1×10^{-10}
Thanet Sand	32·0	0·0	16·0	Small strains (Table 8)	0·2	Drained

Table 7. Mohr–Coulomb parameters for soils in Moorhouse analyses

4.3 Results – short term

Figure 17 shows horizontal wall movement predicted by different analyses for the stage when the wall is acting as a cantilever (Figure 17(a)) and for the stage when the final excavation depth has been reached (Figure 17(b)). Again, because of predominantly undrained conditions, the behaviour is dominated by the shear stiffness in the soil. The mobilised range of elastic deviatoric strain behind the wall is 0·1–1% at both stages. This again indicates that the soil stiffness degrades very quickly from the beginning of excavation and the wall movements for the majority of excavation are governed by stiffness changes in the non-linear range. However, differences between the various predictions are much more pronounced than in the previous case of tunnel excavation.

In this respect the smallest horizontal wall movements are predicted using the non-linear anisotropic stiffness model. As this is the predominant direction of wall movement, the high directional horizontal stiffness that the model employs in this strain range prevents larger deformations. The effect of the E'_h/E'_v stiffness ratio, α, is also more pronounced compared to the tunnelling case, in particular at deeper excavation levels. At the final excavation stage in Figure 17(b), analyses with a varying stiffness ratio produce on average 17·5% higher maximum wall movement (61·8 mm) than the analyses with a constant stiffness ratio (52·6 mm).

Analyses employing the isotropic non-linear stiffness model predict larger wall movements, the largest being the one that utilises the 'previous soft' parameters. The maximum wall movement from this analysis (95·4 mm) is 80% higher than that predicted from analyses with an anisotropic non-linear model and constant stiffness ratio. The shear stiffness for this model (see Figure 3) is the smallest in the working strain range for this problem (0·1–1%).

Similar relationships between the various predictions can also be seen in the profiles of ground surface settlements behind the wall, presented in Figures 18(a) and 18(b) for the cantilever and final stage of excavation respectively, and for the 80 m distance behind the wall (for clarity, the whole lateral extent of the mesh of 200 m is not presented).

4.4 Results – long term

After the excavation is fully completed under undrained conditions, a period of time is allowed in all analyses for full dissipation of excess pore-water pressures. For brevity, only the ground surface settlement profiles are presented in the long term in Figure 19. It is interesting to note that the three analyses with isotropic non-linear stiffness properties predict slight heave beyond the 50 m distance from the wall, whereas this is not the case when anisotropic non-linear stiffness is utilised. In general, the patterns between different predictions are not as clear as in the short-term predictions, most likely due to the interplay between the bulk and the shear stiffness. However, the maximum

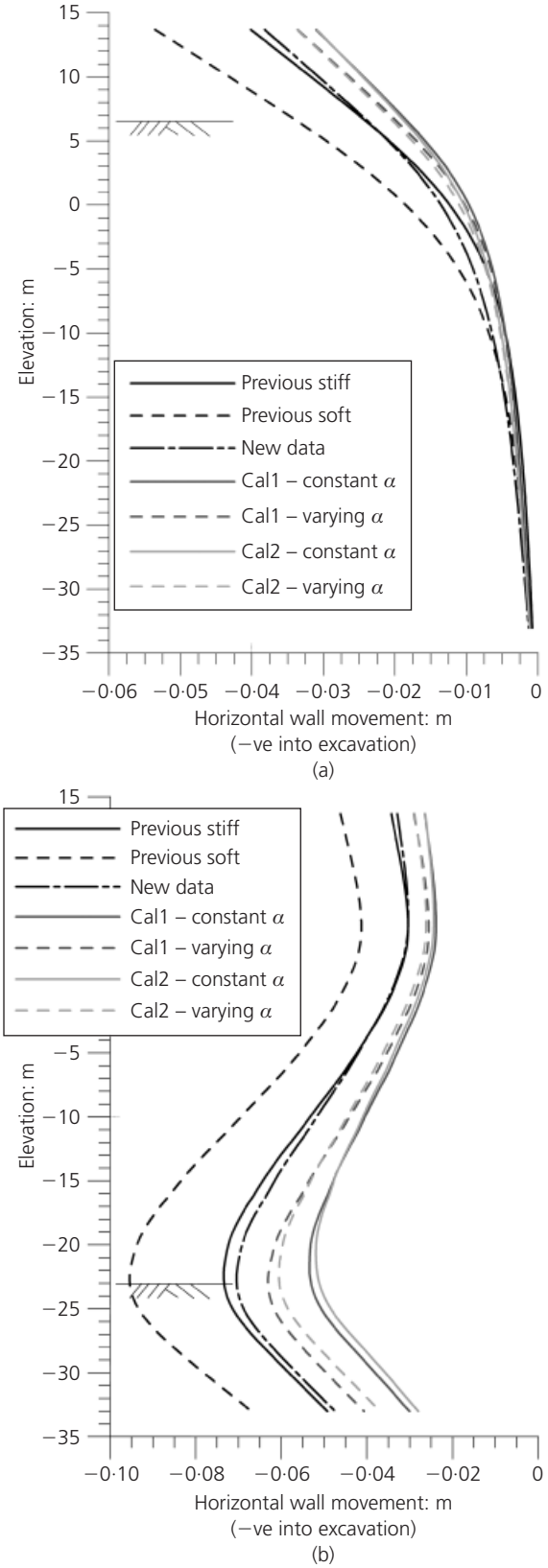

Figure 17. Predicted short-term horizontal wall movement: (a) stages after cantilever; (b) and final excavation stage

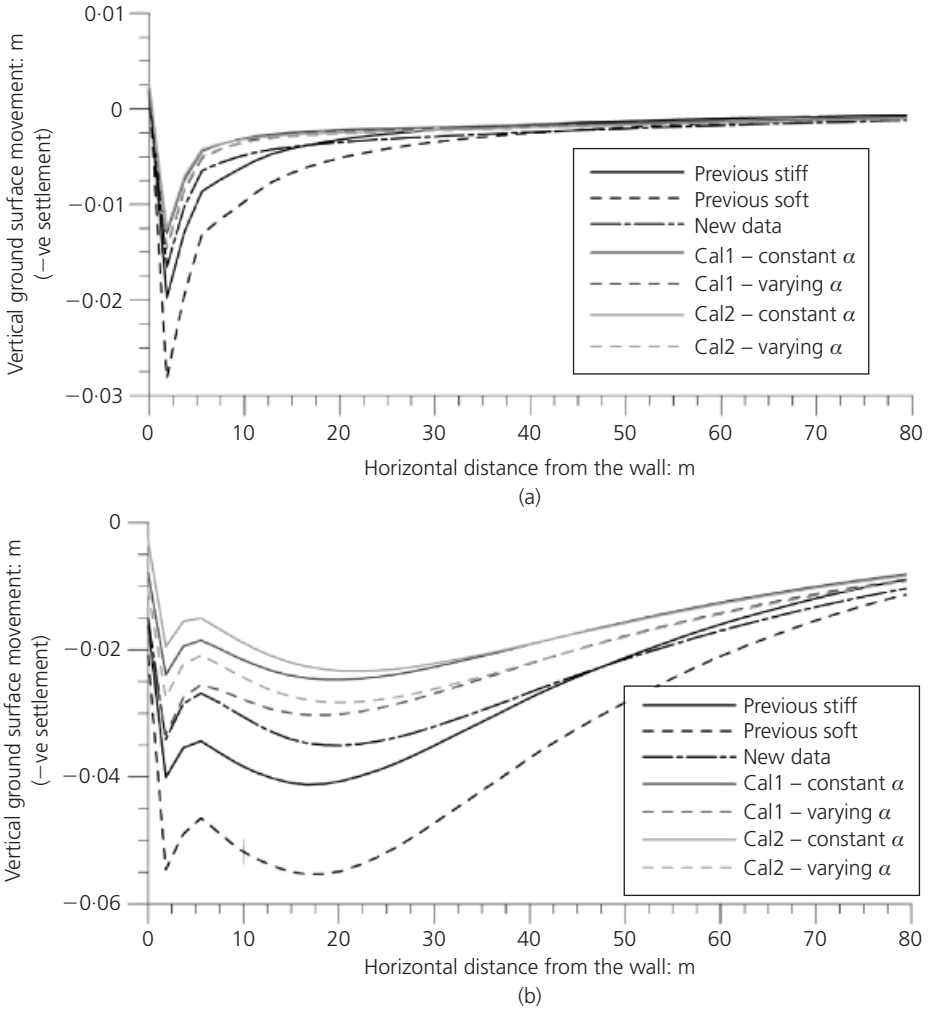

Figure 18. Predicted short-term ground surface settlements behind the wall at: (a) cantilever stage and (b) final excavation stage

difference in predicted surface settlements up to a distance of 20 m behind the wall is about 33%.

5. Conclusion

Recent research on the advanced characterisation of the behaviour of London Clay produced some new insights into the small-strain stiffness properties of this soil. In particular, the isotropic stiffness was shown to be different from that derived in the past from commercial experiments. Additionally, the parameters describing the anisotropic elastic stiffness have been carefully measured and interpreted.

The objective of the study presented in this paper was to investigate the effects of these new data for small-strain stiffness of London Clay on predictions of ground movements in numerical analyses and to compare the results with those obtained using the previously established data. Analyses for each of the two boundary value problems considered differed only in the small-strain stiffness properties employed for London Clay. The following conclusions can be drawn from the presented case studies.

Tunnelling

- The isotropic non-linear shear stiffness calibrated from the new data, with a smaller plateau magnitude but larger plateau, and with more gradual non-linear degradation compared to the previous data, predicts a shallower and wider short-term settlement trough compared to that predicted by the previously established isotropic non-linear shear stiffness of London Clay.
- Using anisotropic non-linear stiffness parameters derived from the new data predicts short-term settlement troughs that are slightly deeper and narrower than that predicted using the isotropic shear stiffness derived from the same data. However,

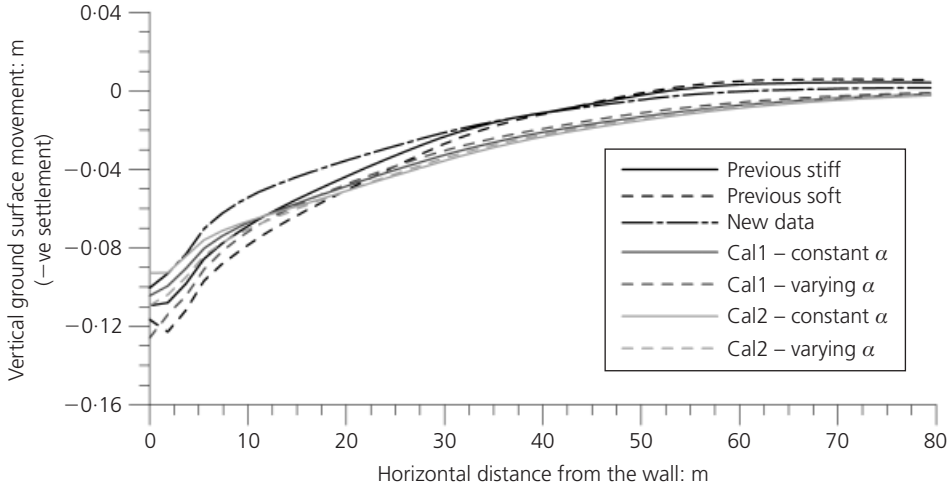

Figure 19. Predicted ground surface settlements behind the wall in the long term

these are still wider and shallower than the two settlement troughs predicted using previously established isotropic non-linear stiffness properties.

- The effect of the stiffness ratio α in the anisotropic non-linear stiffness model (i.e. whether it is constant or varying) is negligible when considering the predicted ground movements in this tunnelling problem.
- In general, the isotropic shear stiffness calibrated from the new data results in the smallest predicted ground movements both in the short and long term.
- The maximum difference between the various analyses in predicting maximum surface settlement is 20% and 26% for the short and long term respectively.

Deep excavation

- Contrary to the tunnelling case, the smallest wall and ground movements in a highly propped deep excavation are predicted using the anisotropic non-linear stiffness properties, due to the high horizontal directional stiffness component.
- The effect of anisotropic stiffness ratio α is more pronounced than in the tunnelling case, in particular in the short term.
- The maximum difference between various analyses in predicting maximum ground movements is 80% and 33% for the short and long term respectively.

In general, for the geotechnical problems considered in this study, the finite-element analyses which employed recently obtained data on the non-linear small-strain stiffness of London Clay predicted smaller ground movements compared to predictions that used previously established stiffness data. Clearly, for any definitive conclusions to be drawn, further investigations are needed on a range of geotechnical problems, in particular those that have some measurements of ground movements.

Acknowledgements

The authors would like to thank Dr Liana Gasparre and Professor Matthew Coop for making their experimental data available to them in a digital format and for allowing their reproduction in this paper. The first author also acknowledges financial support from the Slovenian Research Agency (ARRS) during her stay at Imperial College where this study was undertaken.

Appendix

Non-linear isotropic small-strain stiffness model

Coefficients in Tables 1, 2, 5 and 8 are fitting parameters used in the following equations to give a variation of tangent shear ($3G/p'$) and bulk (K/p') stiffness with both stress and strain level

$$X = \log_{10}\left(\frac{\varepsilon_{\mathrm{d}}}{C\sqrt{3}}\right) \text{ and } Y = \log_{10}\left(\frac{|\varepsilon_{\mathrm{vol}}|}{T}\right)$$

$$\frac{3G}{p'} = A + B\cos(\alpha X^{\gamma}) - \frac{B\alpha\gamma X^{\gamma-1}}{2{\cdot}303}\sin(\alpha X^{\gamma})$$

$$\frac{K}{p'} = R + S\cos(\delta Y^{\eta}) - \frac{S\delta\eta Y^{\eta-1}}{2{\cdot}303}\sin(\delta Y^{\eta})$$

Non-linear anisotropic small-strain stiffness model

Coefficients in Table 3 are fitting parameters used in the following equation to give a variation of tangent drained vertical Young's modulus (E'_{v}/p') with both stress and strain level

Shear stiffness	A	B	$C \times 10^{-4}$: %	α	γ	$\varepsilon_{d,min} \times 10^{-4}$: %	$\varepsilon_{d,max}$: %	G_{min}: kPa
Thanet Sand	930	1120	2	1·100	0·700	3·6373	0·1645	2000
Terrace Gravel	1104	1035	5	0·974	0·940	8·83346	0·3464	2000
Bulk stiffness	R	S	$T \times 10^{-3}$: %	δ	η	$\varepsilon_{vol,min} \times 10^{-3}$: %	$\varepsilon_{vol,max}$: %	K_{min}: kPa
Thanet Sand	190	110	1	0·975	1·010	1·1	0·2	5000
Terrace Gravel	275	225	2	0·998	1·044	2·1	0·2	5000

Table 8. Shear and bulk stiffness parameters for isotropic non-linear elastic model for Terrace Gravel and Thanet Sand in Moorhouse analyses (see Appendix)

Element	Young's modulus, E: kPa	Poisson ratio, μ	Cross-sectional area, A: m^2	Second moment of inertia, I: m^4
Wall (beam elements)	$28{\cdot}0 \times 10^6$	0·2	1·2	0·144
Props (bar elements)	$3{\cdot}0 \times 10^6$	0·2	1·0	—

Table 9. Parameters for wall and prop linear elastic models in Moorhouse analyses

$$Z = \log_{10}\left(\frac{\varepsilon_d}{D\sqrt{3}}\right)$$

$$\frac{E'_v}{p'} = P + Q\cos\left(\beta Z^{\xi}\right) - \frac{Q\beta\xi Z^{\xi-1}}{2{\cdot}303}\sin\left(\beta Z^{\xi}\right)$$

Using input parameters E'_v, μ'_{hh} and α, the remaining cross-anisotropic elastic parameters are calculated as (Graham and Houlsby, 1983)

$$E'_h = \alpha^2 E'_v$$

$$G_{hv} = \frac{\alpha\, E'_v}{2(1+\mu'_{hh})}$$

$$G_{hh} = \frac{E'_h}{2(1+\mu'_{hh})}$$

$$\mu'_{vh} = \mu'_{hh}/\alpha$$

$$\mu'_{hv} = \mu'_{vh}\,\frac{E'_h}{E'_y}$$

Permeability model

The coefficient of permeability k is assumed to be related to the mean effective stress p' through the following equation (Vaughan, 1994)

$$k = k_o\, e^{-ap'}$$

where for London Clay $a = 0{\cdot}007$ and $k_o = 2 \times 10^{-9}$ m/s.

REFERENCES

Addenbrooke TI, Potts DM and Puzrin AM (1997) The influence of pre-failure soil stiffness on the numerical analysis of tunnel construction. *Géotechnique* **47(3)**: 693–712.

Baudet B and Stallebrass S (2004) A constitutive model for structured clays. *Géotechnique* **54(4)**: 269–278.

Franzius JN, Potts DM and Burland JB (2005) The influence of soil anisotropy and K_o on ground surface movements resulting from tunnel excavation. *Géotechnique* **55(3)**: 189–199.

Gasparre A (2005) *Advanced Laboratory Characterisation of London Clay*. PhD thesis, Imperial College London, UK.

Gasparre A, Nishimura S, Minh NA, Coop MR and Jardine RJ (2007) The stiffness of natural London Clay. *Géotechnique* **57(1)**: 33–47.

Graham J and Houlsby GT (1983) Anisotropic elasticity of a natural clay. *Géotechnique* **33(2)**: 165–180.

Grammatikopoulou A, Zdravković L and Potts DM (2006) General formulation of two kinematic hardening constitutive models with a smooth elasto-plastic transition. *International Journal of Geomechanics, ASCE* **6(5)**: 291–302.

Grammatikopoulou A, St John HD and Potts DM (2008) Non-linear and linear models in design of retaining walls. *Proceedings of the Institution of Civil Engineers – Geotechnical Engineering* **161(6)**: 311–323.

Higgins KG, Potts DM and Mair RJ (1996) Numerical modelling of the influence of the Westminster Station excavation and tunnelling on Big Ben clock tower. In *Proceedings of the International Symposium on Geotechnical Aspects of Underground Construction in Soft Ground, London, UK* (Mair RJ and Taylor RN (eds)). Balkema, Rotterdam, the Netherlands, pp. 525–530.

Hight DW and Higgins KG (1994) An approach to the prediction of ground movements in engineering practice: background and application. In *Proceedings of the International Symposium on Pre-failure Deformation of Geomaterials, Hokkaido, Japan* (Shibuya S, Mitachi T and Miura S (eds)). Balkema, Rotterdam, the Netherlands, pp. 909–945.

Hight DW, Gasparre A, Nishimura S *et al.* (2007) Characteristics of the London Clay from the Terminal 5 site at Heathrow Airport. *Géotechnique* **57(1)**: 3–18.

Jardine RJ, Potts DM, Fourie AB and Burland JB (1986) Studies of the influence of non-linear stress–strain characteristics in soil–structure interaction. *Géotechnique* **36(3)**: 377–396.

Kanapathipillai A (1996) *Review of the BRICK Model of Soil Behaviour*. MSc thesis, Imperial College, London, UK.

Kavvadas M and Amorosi A (2000) A constitutive model for structured soils. *Géotechnique* **50(3)**: 263–273.

Lambe TW (1973) Predictions in soil engineering. *Géotechnique* **23(2)**: 149–202.

Mair RJ (2008) Tunnelling and geotechnics: new horizons. *Géotechnique* **58(9)**: 695–736.

Manzari MT and Dafalias YF (1997) A critical state two-surface plasticity model for sands. *Géotechnique* **47(2)**: 255–272.

Potts DM and Zdravković L (1999) *Finite Element Analysis in Geotechnical Engineering: Theory*. Thomas Telford, London, UK.

Potts DM and Zdravković L (2001) *Finite Element Analysis in Geotechnical Engineering: Application*. Thomas Telford, London, UK.

Schroeder FC, Higgins KG, Wright P and Potts DM (2011) Assessment of overbridge openings on the London Underground tunnel network. *Proceedings of the 15th European Conference on Soil Mechanics and Geotechnical Engineering– XV ECSMGE, Athens, Greece*, pp. 1733–1738.

Simpson B (1992) Retaining structures: displacement and design. *Géotechnique* **42(4)**: 541–576.

Simpson B, O'Riordan NJ and Croft DD (1979) A computer model for the analysis of ground movements in London Clay. *Géotechnique* **29(2)**: 149–175.

Simpson B, Atkinson JH and Jovičić V (1996) The influence of anisotropy on calculations of ground settlements above tunnels. In *Proceedings of the International Symposium on Geotechnical Aspects of Underground Construction in Soft Ground, London, UK* (Mair RJ and Taylor RN (eds)). Balkema, Rotterdam, the Netherlands, pp. 591–594.

Stallebrass SE, Jovičić V and Taylor RN (1994) Short term and long term settlements around a tunnel in stiff clay. In *Proceedings of the 3rd European Conference on Numerical Methods in Geotechnical Engineering, Manchester, UK* (Smith IM (ed.)). Balkema, Rotterdam, the Netherlands, pp. 235–240.

Standing JR, Nyren RJ, Burland JB and Longworth TI (1996) The measurement of ground movement due to tunnelling at two control sites along the Jubilee Line Extension. In *Proceedings of the International Symposium on Geotechnical Aspects of Underground Construction in Soft Ground, London, UK* (Mair RJ and Taylor RN (eds)). Balkema, Rotterdam, the Netherlands, pp. 751–756.

Vaughan PR (1994) Assumption, prediction and reality in geotechnical engineering. *Géotechnique* **44(4)**: 573–603.

Zdravković L, Potts DM and St John HD (2005) Modelling of a 3D excavation in finite element analysis. *Géotechnique* **55(7)**: 497–513.